Luminescence characteristics of chromium-doped by high-temperature diffusion CVD−ZnSe

© V.P. Kalinushkin[1], A.A. Gladilin[1], O.V. Uvarov[1], S.A. Mironov[1,¶], N.N. Ilichev[1], M.I. Studenikin[1], M.S. Storozhevykh[1], E.M. Gavrishchuk[2], V.B. Ikonnikov[2], N.A. Timofeeva[2]

[1] Prokhorov Institute of General Physics, Russian Academy of Sciences, 119991 Moscow, Russia
[2] Devyatykh Institute of Chemistry of High-Purity Substances, Russian Academy of Sciences, 603951 Nizhny Novgorod, Russia

[¶] E-mail: sa.mironov@kapella.gpi.ru

Received June 1, 2022
Revised August 22, 2023
Accepted August 28, 2023

Using two-photon confocal microscopy in the spectral range of $0.44-0.73\,\mu$m, the spatial distribution of the luminescent characteristics of CVD-ZnSe doped with chromium using the HIP process was studied. It has been established that as a result of this process, four types of impurity-defect centers are formed in the crystal. It is shown that their formation involves point centers that form in the doping zone and diffuse deep into the crystal. Assumptions are made about the nature of these point centers.

Keywords: zinc selenide, two-photon confocal microscopy, semiconductors, defects.

DOI: 10.61011/SC.2023.06.57168.3886

1. Introduction

Polycrystals of zinc selenide grown by chemical deposition from the gas phase (CVD-ZnSe) and doped with Fe^{2+} and Cr^{2+} ions by high-temperature diffusion are used as active media of IR lasers ($2-5\,\mu$m) [1–3]. Currently, high generation characteristics of lasers have been achieved using semiconductor crystals $Fe^{2+}:ZnSe$ and $Cr^{2+}:ZnSe$ [4,5]. However, further scaling of the output characteristics of such lasers is limited by a number of reasons. The critical characteristics of these media — optical transmission, absorption and luminescence — depend not only on the nature and concentration of the alloying component and its distribution in the matrix, but largely on the nature of intrinsic or impurity defects of the base material. Such imperfections are determined by the conditions of crystal growth, as well as their subsequent high-temperature treatment used for alloying with transition metal ions.

Thus, the study of the nature of defects and the patterns of their formation at all stages of the manufacture of an optically active medium is a necessary step in the development of optimal laser element technology $Fe^{2+}(Cr^{2+}):ZnSe$.

Luminescence is one of the widely used methods for studying the impurity-defect composition of semiconductors. Therefore, studies of the spatial distribution of the luminescent characteristics of doped crystals are of great interest. An effective method for studying the spatial distribution of luminescent characteristics is two-photon confocal microscopy (TPCM). This technique makes it possible to register the photoluminescence (PL) spectra not only on the surface, but also in the volume of the sample under study, and allows us to correlate the nature of the change in the centers of the ZnSe polycrystal with the concentration profile of the alloying element [6,7]. Using the TPCM method, it was revealed that diffusion doping of CVD-ZnSe with Fe^{2+} ions leads to the formation of additional impurity-defect centers (IDC) formed on point defects [8–10]. At the same time, areas with increased luminescence intensity of these IDC are recorded, having the form of bands with width about hundreds of μm that depends on the annealing time. These strips are parallel to the plane from which the alloying was carried out. The first results of the use of TPCM for the study of polycrystals $Cr^{2+}:ZnSe$ are presented in papers [8,11]. In particular, in the work of [11] it was reported that regions similar to areas with increased luminescence intensity were also observed in ZnSe crystals doped with chromium. This article is a continuation of these works.

2. Experiment procedure

Samples of high-purity and chromium-doped from the surface of the film were used under conditions of CVD-ZnSe hot isostatic pressing (HIP-treatment) to study the spatial distribution of PL. The initial samples had the shape of parallelepipeds with the size $15\times10\times5$ mm. The chromium film was applied by electron beam evaporation on one side of the sample. The following HIP-processing modes were used: $P = 1000$ atm, $t = 28-38.5$ h, $T = 1240-1250°$s. The surfaces of the samples were mechanically polished with abrasive diamond synthetic powder before the measurements.

Studies by the TPCM method were carried out on a confocal microscope of Carl Zeiss LSM 710 NLO. Two-photon excitation was performed by a laser with a tunable wavelength in the range $0.71-1.05\,\mu$m (in this

work, radiation with a wavelength of 0.8 μm was used). The pulse duration was 150 femtoseconds, frequency — 80 MHz, maximum average power — 0.5 W. Luminescence spectra were recorded at room temperature in the range 440−725 nm with a spectral resolution of 10 nm. The equipment used allows recording „flat“ and „volumetric“ luminescence maps in the specified spectral range at distances from the surface up to 3 mm. A detailed description of the technique is provided in [6,7].

Samples of zinc selenide doped with chromium were studied in this work. The study was carried out from a chip perpendicular to the surface from which the alloying took place. The concentration of Cr^{2+} varied along the cleavage surface. This experimental setup allows measuring the dependence of the concentration of Cr^{2+} on the distance from the doping surface, as well as the dependence of the luminescence intensity on the concentration of Cr^{2+}, excluding the influence of a highly defective area of the crystal surface.

The distribution of the concentration of active ions Cr^{2+} along the direction of the diffusion flow was calculated based on data on the absorption of radiation at a wavelength of 1.7 μm. HYPERION 2000 IR microscope was used for this purpose in combination with the Tenzor-27 IR Fourier spectrometer (Bruker). A detailed description of the scanning technique is presented in [12,13].

In this article, the assumption is investigated that the PL spectrum obtained using TPCM consists of several folded lines, which significantly complicates the interpretation of the results, in frequency the spatial distribution of the bands PL. This paper proposes a method for decomposing the spectrum into lines taking into account the spatial distribution of spectral lines and the influence of crystal grain boundaries on this distribution, as well as the dependence of the intensity of the PL on the pumping power and behavior.

The spatial distribution of the intensity of the selected spectral lines was constructed by 20 points. The point size was $\sim 30 \times 30\,\mu$m, step — 200 μm. The initial PL spectrum was obtained using the TPCM at a depth of 200 μm from the chip surface to exclude the influence of the polycrystal surface.

3. Results and discussion

Figure 1, *b* and *d* show „flat“ PL maps at wavelengths 473 nm (*b*) and 521 nm (*d*), registered in the sample of the original CVD-ZnSe at a depth of 100 μm.

Luminescent contrast allows visualization of polycrystalline ZnSe microstructure with grain size $\sim$20−50 μm. Luminescence intensity inside the grains significantly varied. Grain boundaries were usually characterized by a low intensity of PL. However, grain boundary regions with high PL intensity were observed in the spectral range from 480 to 725 nm, the so-called impurity-defect range. The spectra were obtained from the regions identified on the „flat“ map (Figure 1, *b* and *d*). Linear dimensions of the selected area on the „flat“ map Figure 1, $b \sim 100\,\mu$m.

An area with a diameter of $\sim 10\,\mu$m with a high intensity of the impurity-defect range (bright points) and an area with a diameter of 100 μm containing bright points are defined in Figure 1, *d*.

With „integral“ registration of PL (with a region with a diameter of $\sim 100\,\mu$m), the emission line 463−473 nm dominates in the spectra (Figure 1, *a*, curves *1*−*3*), which in the works of [8,9] was associated with exciton radiation, and there is IDC luminescence with weak intensity (in $\sim$ 500 times weaker) — a wide band with a maximum intensity near 521 nm and a long-wave tail up to 620 nm. PL line with weaker intensity (at the threshold of sensitivity of the equipment) in the range from 620 to 725 nm are also observed, the so-called „red lines“ (see the insert in Figure 1, *a*).

The curve *S* (thick solid line) is the addition of curves *P* (solid lines) with a Gaussian profile and maxima of about 521, 565, 608 nm, as well as in the range of red lines — 638, 667 and 706 nm.

The composition of the spectrum shown in Figure 1, *c* does not differ from the regions considered above. At the same time, the spectrum obtained from the region 1 (Figure 1, *d*) is dominated by a PL band with a maximum near the wavelength of 521 nm (Figure 1, *b*) and a long-wave tail up to 580 nm. This band *S* can be represented as the sum of lines *P* with wavelengths of 520, 556 nm and less intense — 581 nm.

The PL line in the same region with a maximum near the wavelength of 473 nm, associated with exciton radiation,has a weaker intensity than the impurity PL in the range 500−580 nm.

It should be noted that the presence of bright dots weakly affects the PL spectrum obtained from a region with a size of 100 μm (Figure 1, *c* and *d*). The luminescent characteristics of the polycrystals under study were sufficiently homogeneous on a macroscopic scale. These results were typical for all samples of undoped CVD−ZnSe studied in this work.

Figure 2 shows the results obtained on the sample Cr^{2+}:ZnSe. Spatial distributions of PL (Figure 2, *a*–*f*, solid line) are obtained from flat maps (Figure 2, *g*–*l*) at wavelengths 473, 483, 500, 560, 628 and 715 nm, respectively. The graphs show the spatial distributions of the lines at the corresponding wavelengths obtained from the decomposition of the spectrum (Figure 2, *a*–*f*, circles), as well as the diffusion concentration profile of the ions Cr^{2+}. (Figure 2, *a*–*f*, dashed dotted line).

According to the above dependencies, the doped sample Cr^{2+}:ZnSe can be divided into three conditional zones (Figure 3, *a*): zone I from the doping surface to 2000 μm, zone II from 2000 to 3000 μm and zone III from 3000 to 4500 μm.

Figure 3, *b* shows the PL spectra (open points) registered in the corresponding regions 1−7 shown on the „flat“ map. Figure 3, *b* (graphs 1−3) shows the spectra recorded in

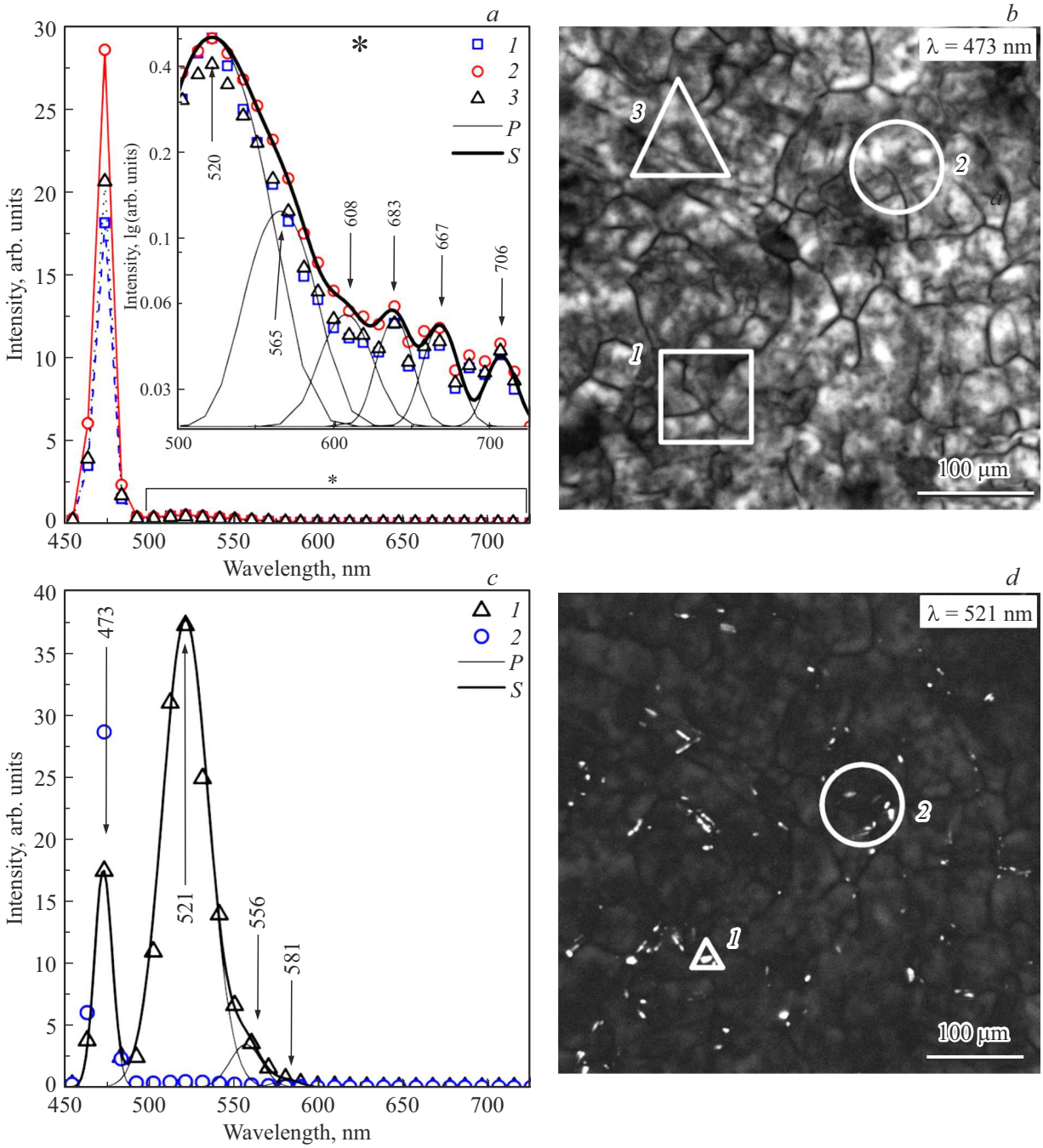

Figure 1. PL spectra (*a*) and (*c*) registered in the sample regions (at a depth of 100 μm from the crystal surface) indicated on „flat" maps (*b*) and (*d*) accordingly. „Flat" maps were obtained at wavelengths 473 nm (*b*) and 521 nm (*d*). Experimental results (open symbols), calculated spectral lines as a result of the decomposition of the experimental spectrum (thin solid lines), and the sum of the calculated spectral lines (thick solid lines) are shown on the PL spectra. The insert (*a*) shows an enlarged part of the spectrum in the range from 500 to 725 nm.

zone I. The decompositions of the spectra on the line (the dashed line) are also given. The concentration of Cr^{2+} decreases from $3 \cdot 10^{18}$ to $2 \cdot 10^{17}$ see^{-3}.

When moving away from the doping surface, the intensity of the wide band begins to grow by more than an order of magnitude, and the maximum shifts to the short-wave part (Figure 3, *a*, graphs 2 and 3). The left wing of the wide band also shifts towards the short wavelengths (possibly closing weak lines observed earlier in this range). The luminescence intensity of the red lines remained at the same level. The wide band is decomposed into two lines with a Gaussian profile with maxima 560–580 and 618 nm (lines 560 and 618 nm). As the distance from the surface increases, the intensity of the line 560 nm increases much faster than

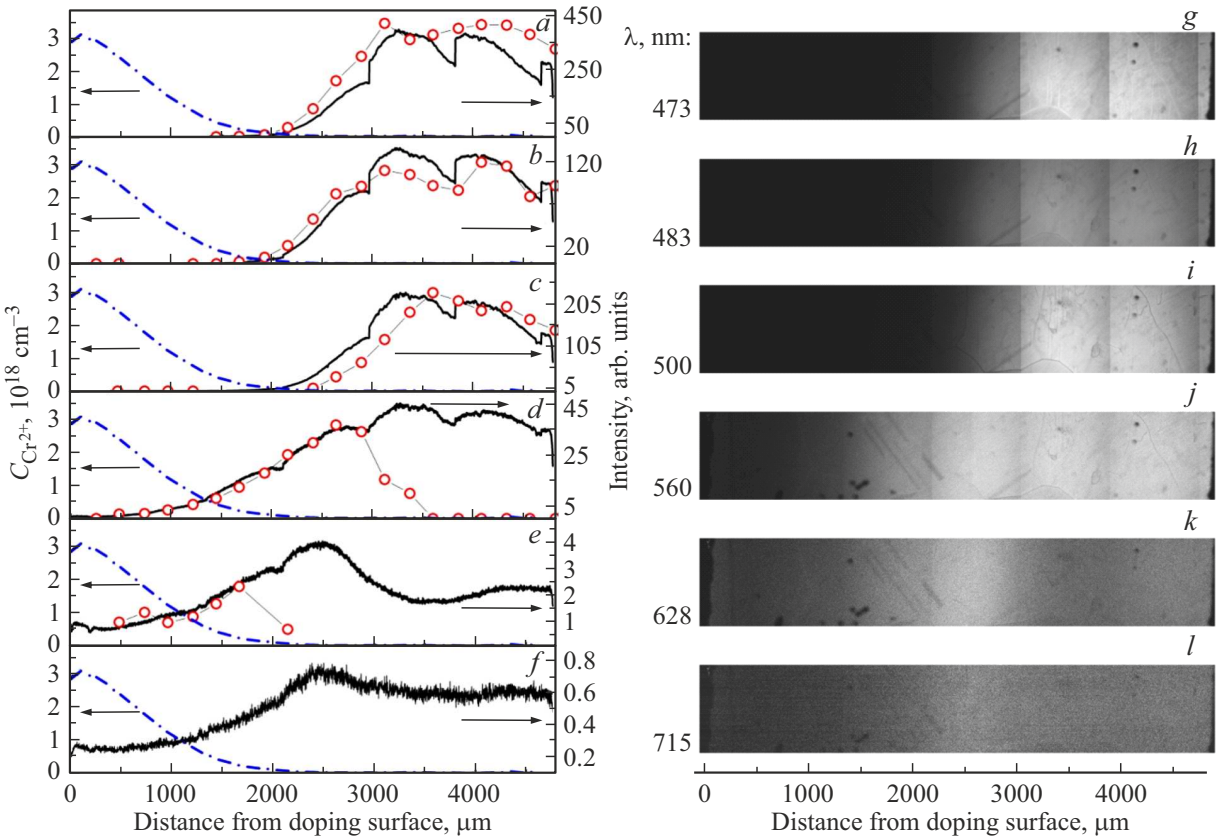

Figure 2. Spatial distributions of PL (solid curve, right *Y*-axis) of the ZnSe : Cr sample obtained from the entire area of „flat" maps at wavelengths 473 (*a, g*), 483 (*b, h*), 500 (*c, i*), 560 (*d, j*), 628 (*e, k*) and 715 nm (*f, l*). The graphs (*a–f*) show the spatial distributions of spectral lines obtained by spectrum decomposition (circles, right *Y*-axis). The distribution of the ion concentration Cr^{2+} (dashed curve, left *Y*-axis) is also demonstrated.

618 nm, in ~ 8 and ~ 2 times, respectively (Figure 2 and 3, *b* (1–3)). As a result, there is a shift of the maximum of the general peak and a shift of its short-wave edge.

The PL spectrum obtained at point 1, which is located near the doping surface, is a wide band in the range from 540 to 660 nm (Figure 3, *b*, graph 1). There is also a weak luminescence in the region of 500 nm and in the range from 680 to 725 nm (red lines).

By the end of the zone I, the maximum intensity of the PL is located at wavelengths in the region of 560 nm, and a glow appears in the spectral region 465–485 nm (Figure 3, *b*, graph 3). The PL band 465 – 485 nm can be decomposed by two narrow lines with a Gaussian profile and maxima in the region of 473 and 483 nm. Luminescence in the region of 500 nm at the edge of the zone I is decomposed by weak (at noise level) lines with maxima 502, 521 and 531 nm, and in the red glow area — lines with maxima 696 and 715 nm.

The chromium concentration falls below the detection threshold in zone II. The PL spectra of this zone and their decomposition are shown in Figure 3, *b* (4, 5). It can be seen that the intensity of the PL lines 473, 483 and 560 nm is growing rapidly. The line 618 nm is not observed in the spectra recorded at distances $> 2200\,\mu$m from the doping surface. Its absence may be due to the fact that the intensity of the long-wave tail of the 560 nm line has become greater than the intensity of the 618 nm line. In addition, a part of the spectrum begins to appear in the middle of zone II, which is approximated by a line with a maximum of 502 nm. Its intensity also increases rapidly with increasing distance from the surface. The intensity of the red lines increases slightly (Figure 2, *e, f*), but on the PL spectra shown in Figure 3, *b* (4, 5), they are not detected due to relatively low intensity.

The presence of Cr^{2+} in zone III is registered at the level of the sensitivity threshold of the equipment. This is most likely from uncontrolled pollution.

The spectra of the PL (circles) of this zone and their decomposition (dashed line) are shown in Figure 3, *b* (6, 7). The luminescence spectrum is decomposed into four main lines 473, 483, 450 and 560 nm. The intensities of the lines 473 and 483 nm are approximately constant with a possible slight decrease at the edge of the sample. The intensity of the PL line 560 nm decreases rapidly with increasing distance from the surface from which the doping took place, and, starting from a depth of $\sim 3500\,\mu$m, it is difficult to separate it from the „tail" line 502 nm. The maximum intensity of the line 502 nm is at a distance of $\sim 3000\,\mu$m

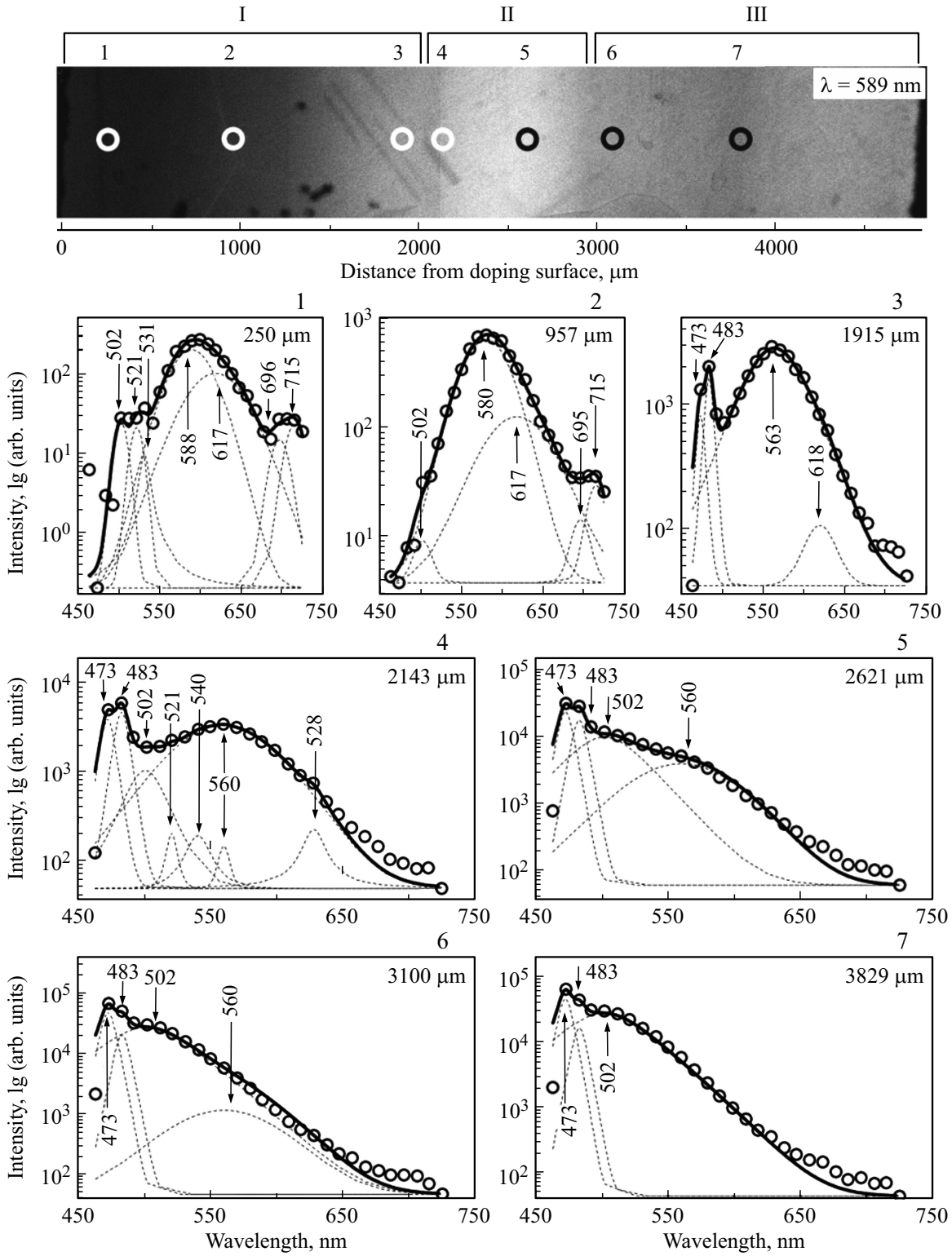

Figure 3. *a* — „flat“ ZnSe:Cr PL map at a wavelength of 589 nm, divided into zones I, II, III. *b* — PL spectra recorded in regions at a distance 250 (1), 957 (2), 1915 (3), 2143 (4), 2621 (5), 3100 (6) and 3829 μm (7) from the doping surface indicated on the „flat“ map (*a*). The spectra show experimental results (circles), calculated spectral lines as a result of the decomposition of the experimental spectrum (dashed curve) and the sum of the calculated spectral lines (thick solid curve).

from the doping surface, then the decline begins (Figure 2, *c* and 3, *b* (6, 7)). The intensity of the red lines does not change (Figure 2, *f*).

It can be seen that the spatial distributions of the PL intensities observed experimentally are close to similar dependences of the spectral lines 473, 483 and 502 nm obtained using mathematical data processing. The spatial dependences of the intensity of these lines are close, and they are practically not affected by other lines (560 and 618 nm). It is possible that a slight decrease in the intensity of the PL of experimentally removed dependences at wavelengths 473 and 483 nm at the edge of the sample is associated with a decrease in the luminescence intensity of the 500 nm line and its short-wave wing.

The situation with spatial dependencies at wavelengths of 570 and 630 nm is more complicated. A maximum of the spatial distribution of luminescence is observed in this experiment at a wavelength of 630 nm at a distance of 2300 μm from the doping surface. There is also a maximum of the line intensity distribution of 560 nm (Figure 2, *d* and *e*). This is attributable to the fact that the impact of the 500 nm line is minimized in the spectral range > 600 nm, whereas in the region of 560 nm it is quite large. So, the intensity of the 500 nm line can exceed the intensity of the 560 nm line by 2 times.

The intensity of the line 618 nm in almost the entire space is less than the intensity of the line 560 nm. As a result, the maximum intensity of the long-wave edge of the line 560 nm is recorded at wavelengths ~ 630 nm.

Special attention is required to study the nature of the intensity distribution of PL of different wavelengths in the grain boundaries Cr^{2+}:ZnSe, which are well visualized on „flat“ maps of PL (Figure 2). It can be seen that around the grains at wavelengths of 473 nm (Figure 2, *g*) an area with increased intensity of PL is observed at wavelengths of 483 nm (Figure 2, *h*) — either the contrast is significantly reduced, or the grain boundary is registered as a narrow line with a reduced intensity of PL. The grain boundary looks like a region with a reduced PL intensity (dark region) at 500 nm wavelength (Figure 2, *i*). The contrast of grain boundaries at a wavelength of 560 nm (Figure 2, *j*) in the crystal region at a depth of up to 2200 μm (i. e., where the 560 nm line is reliably recorded) is absent and begins to appear at large distances from the doping surface, showing a weak intensity of PL. There is no luminescent contrast at the grain boundaries throughout the sample at 630 and 715 nm wavelengths (Figure 2, *k* and *l*).

The observed difference in the luminescence of grain boundaries at wavelengths of 473 and 483 nm indicates the different nature of the centers responsible for this glow. This is confirmed by the results of [14], where it was shown that the intensities of PL lines with wavelengths of 473 and 483 nm have a different dependence on the pumping power. Thus, the intensity of the PL of the 473 nm line was proportional to the 4th degree of pumping power, and the 483 nm line was proportional to the 2nd degree of this power. This means that the 473 nm line is attributable to exciton recombination in accordance with the data of the work [15] and the 483nm line is attributable to recombination through the IDC. Thus, the proposed decomposition of luminescence in the spectral range 465−485 nm into two lines is justified.

The decomposition of the spectra in the range 490−660 nm into three lines is confirmed by the following facts. It can be seen from the spectra and luminescence of the grain boundaries that luminescence in zones II and III in the spectrum ranges 490−540 nm and 600−725 nm is determined by IDC of different nature. The IDC forming the 500 nm line (IDC-500) are apparently captured by grain boundaries. Therefore, a region with a reduced concentration of these IDC is formed around them, and, as a consequence, a reduced intensity of PL in the range 490−540 nm.

The IDC forming the lines 560 nm (IDC-560) and 618 nm (IDC-618), apparently, are not connected with grain boundaries. Therefore, there is no contrast at the grain boundaries in the spectral range > 570 nm where the impact of the 500 nm line is reduced. The decomposition of the PL spectra in zone I into two lines is necessary to explain the experimentally observed shift of luminescence into the short-wavelength region.

The results obtained show that the PL radiation in crystals Cr^{2+}:ZnSe at wavelengths 473 and 483 nm, as in the case of doping Fe^{2+} [9,10], is suppressed in a zone with a high concentration of ions Cr^{2+} and is recorded in parts of the crystal in which the dopant content is less than the sensitivity used. Such an effect Cr^{2+} was observed in previous studies [16–18].

The spatial distribution of the intensity of the PL line with a wavelength of 560 nm leads to the formation of an area with increased luminescence intensity with a maximum at a depth of 2300 mm. The spatial distribution of the intensity of PL lines with a wavelength of 500 nm leads to the formation of an area with increased luminescence intensity with a maximum at a depth of 3800 mm. Both areas with increased luminescence intensity have a spatial width of $\sim 500-600$ μm. The spatial intensity distribution of the PL line with a wavelength of 483 nm does not form areas with increased luminescence intensity in this sample. Its intensity at a distance of 3000 μm from the doping surface most likely reaches a plateau. A slight decrease at the end of zone III (at the surface opposite to the doping surface) may be associated with contamination of this zone with chromium or the effect of a decrease in the intensity of the PL line at a wavelength of 500 nm. The PL line at a wavelength of 618 nm is observed in a part of the crystal with a high concentration of chromium $C_{Cr}^{2+}) \sim 10^{18}$ cm^{-3}. However, the luminescence intensity of the 618 nm line does not correlate with the chromium concentration. Red lines were also recorded in the source material. They do not form a reliably fixed areas with increased luminescence intensity in the sample studied in this work Cr^{2+}:ZnSe, unlike an alloyed crystal with a ZD-ZnSe:Fe.

Note that the lines 483, 500 and 618 nm were not observed in the initial polycrystals. A line with a maximum intensity of 560 nm in the initial CVD-ZnSe is recorded, but the intensity of its luminescence is very small (by ~ 2 orders of magnitude less than the luminescence intensity of the 560 nm line in Cr^{2+}:ZnSe). Thus, it can be argued that as a result of diffusion doping with CD-ZnSe chromium under HIP conditions, IDC are formed in polycrystals, leading to the formation of the following lines in the PL spectrum: 483 nm (IDC-483), 500 nm (IDC-500), 560 nm (IDC-560), 618 nm (IDC-618). In this case, the lines 560 and 500 nm form standard areas with increased luminescence intensity. Therefore, it can be concluded that IDC-560 and IDC-500 are formed, as in the case of Fe^{2+}:ZnSe, in the near-surface layers of the sample, from where the diffusion flow of the dopant comes, and then it diffuses into the depth of the sample. However, areas with increased luminescence intensity form lines with maxima near 540 nm and red lines in Fe^{2+}:ZnSe. Thus, the processes of iron doping in the atmosphere Ar (1 atm) at a temperature of 1000°C and chromium doping processes under HIP-processing conditions lead to significantly different results in the composition of IDC.

Lines with intensity maxima of 500 and 560 nm were observed in [19] and associated with IDC with an excess of selenium. This suggests that chromium alloying of CVD-ZnSe crystals under HIP treatment conditions leads to the formation of excess selenium in the sample layers bordering the source of the alloying impurity. This leads to the diffusion of intrinsic defects (interstitial selenium and zinc vacancies) into the crystal volume, their interaction with residual impurities and the formation of IDC-500 and IDC-560.

It is not possible to determine the nature and real spatial distribution of IDC-483. It is possible that IDC-483 are distributed relatively evenly over the sample, but recombination through them (as well as the luminescence of excitons with a wavelength of 473 nm) is suppressed in the I zone due to the high concentration of Cr^{2+} ions in it, as well as IDC-500 and IDC-560.

4. Conclusion

In conclusion let's summarize the main results and findings of the performed study.

1. As a result of diffusion doping with CD-ZnSe ions Cr^{2+} under HIP treatment conditions ($T = 1200$°C), at least four new types of IDC are formed in the polycrystal: IDC-483, IDC-500, IDC-560, IDC-618.

2. Defects, which are part of the two centers of IDC-500 and IDC-560, are formed in the doping zone and diffuse into the depths of the crystal.

3. The near-surface region of the crystal from which the doping proceeds has an increased concentration of selenium. Most likely, IDC-500 and IDC-560 are associated with zinc vacancies and interstitial selenium.

Funding

The study was performed under State assignment No. 0024-2019-0001. The study was performed using the equipment of the center for collective use „Analytical Center of General Physics Institute of the Russian Academy of Sciences".

Conflict of interest

The authors declare that they have no conflict of interest.

References

[1] S.B. Mirov, V.V. Fedorov, D. Martyshkin, I.S. Moskalev, M. Mirov, S. Vasilyev. IEEE J. Select. Top. Quant. Electron., **21** (1), 1601719 (2015). 10.1109/JSTQE.2014.2346512
[2] S. Vasilyev, I. Moskalev, M. Mirov, V. Smolski, D. Martyshkin, V. Fedorov, S. Mirov, V. Gapontsev. Proc. SPIE, **10193**, 101930U (2017).
[3] S.V. Kurashkin, O.V. Martynova, D.V. Savin, E.M. Gavrishchuk, S.S. Balabanov, V.B. Ikonnikov, V.V. Sharkov. Phys. Lett., **16** (17), 075801 (2019). https://doi.org/10.1088/1612-202X/ab21cd
[4] A.E. Dormidonov, K.N. Firsov, E.M. Gavrishchuk, V.B. Ikonnikov, S.Y. Kazantsev, I.G. Kononov, T.V. Kotereva, D.V. Savin, N.A. Timofeeva. Appl. Phys. B, **122**, 211 (2016). https://doi.org/10.1007/s00340-016-6489-6
[5] M.P. Frolov, Yu.V. Korostelin, V.I. Kozlovsky, Ya.K. Skasyrsky. Laser Phys., **29** (8), 085004 (2019). https://doi.org/10.1088/1555-6611/ab2be3
[6] V.P. Kalinushkin, O.V. Uvarov, A.A. Gladilin. J. Electron. Mater., **47** (9), 5087 (2018). https://doi.org/10.1007/s11664-018-6393-4
[7] V.P. Kalinushkin, O.V. Uvarov. ZhTF, **86** (12), 119 (2016). (in Russian).
[8] E.M. Gavrishchuk, A.A. Gladilin, V.P. Danilov, V.B. Ikonnikov, N.N. Il'ichev, V.P. Kalinushkin, A.V. Ryabova, M.I. Studenikin, N.A. Timofeeva, O.V. Uvarov, V.A. Chapnin. Inorg. mater., **52** (11), 1180 (2016). (in Russian). https://doi.org/10.7868/S0002337X16110014
[9] S.S. Balabanov, E.M. Gavrishchuk, A.V. Gladilin, V.B. Ikonnikov, N.I. Ilyichev, V.P. Kalinushkin, S.A. Mironov, D.V. Savin, M.I. Studenikin, N.A. Timofeeva, O.V. Uvarov, V.A. Chapnin. Inorg. mater., **55** (5), 459 (2019). (in Russian). https://doi.org/10.1134/S0002337X19050014
[10] V. Kalinushkin, O. Uvarov, S. Mironov, K. Nartov, N. Il'ichev, M. Studenikin, E. Gavrischuk, N. Timofeeva, S. Rodin, A. Gladilin. J. Luminesc., **231**, 117795, (2021). https://doi.org/10.1016/j.jlumin.2020.117795.
[11] A. Gladilin, O. Uvarov, S. Mironov, N. Timofeeva, E. Gavrischuk, V. Kalinushkin. Acta Phys. Polon. A, **136** (4), 637 (2019). https://doi.org/10.12693/APhysPolA.136.637
[12] K.N. Firsov, E.M. Gavrishchuk, V.B. Ikonnikov, S.Yu. Kazantsev, I.G. Kononov, S.A. Rodin, D.V. Savin, N.A. Timofeeva. Laser Phys. Lett., **13** (1), 015001 (2016). https://doi.org/10.1088/1612-2011/13/1/015001
[13] T.V. Kotereva, V.B. Ikonnikov, E.M. Gavrishchuk, A.M. Potapov, D.V. Savin. ZhTF, **88** (7), 1110 (2018). (in Russian). https://doi.org/10.21883/JTF.2018.07.46189.2572

[14] V.P. Kalinushkin, A.A. Gladilin, O.V. Uvarov, S.A. Mironov, N.N. Ilyichev, M.I. Studenikin, V.A. Chapnin, N.A. Timofeeva, E.M. Gavrishchuk, S.A. Rodin, V.B. Ikonnikov, G.G. Novikov. FTP, **55** (5), 410 (2021). (in Russian). https://doi.org/10.21883/FTP.2021.05.50829.9614
[15] A.A. Gladilin, V.P. Danilov, N.N. Ilyichev, V.P. Kalinushkin, M.I. Studenikin, O.V. Uvarov, V.A. Chapnin, A.V. Ryabova, A.V. Sidorin, E.S. Gulyamova, V.V. Tumorin, P.P. Pashinin. FTP, **54** (1), 48 (2020). (in Russian). https://doi.org/10.21883/FTP.2020.01.48770.9143
[16] L.L. Kulyuk, R. Laiho, A.V. Lashkul, E. Lahderanta, D.D. Nedeoglo, I.V. Radevici. Physica B, **405**, 4330 (2010). https://doi.org/10.1016/j.physb.2010.07.036
[17] M. Surma, M. Godlewski, T.R. Surkova. Phys. Rev. B, **50**, 8319 (1994). https://doi.org/10.1103/PhysRevB.50.8319
[18] M. Tabei, S. Shionoya, H. Ohmatsu. Jpn. Appl. Phys., **14**, 240 (1975). https://doi.org/10.1143/JJAP.14.240
[19] V.P. Kalinushkin, A.A. Gladilin, O.V. Uvarov, S.A. Mironov, V.A. Chapnin, M.I. Studenikin, N.N. Ilyichev, E.M. Gavrishchuk, S.A. Rodin, N.A. Timofeeva. FTP, **56** (1), 410 (2022). (in Russian). https://doi.org/10.21883/FTP.2021.05.50829.9614

Translated by A.Akhtyamov